

## SEAFLOOR POSITIONING MODEL FOR SIMULTANEOUS ESTIMATION OF SOUND VELOCITY

Shengqiu Zhang<sup>1</sup>, Tianhe Xu<sup>2\*</sup>, Xianping Qin<sup>3</sup>

<sup>1</sup> College of Geology Engineering and Geomatics, Chang'an University, Xi'an 710054, Shanxi, China – shengqiuz@163.com

<sup>2</sup> Institute of Space Science, Shandong University, Weihai 264209, Shandong, China – thxugfz@163.com

<sup>3</sup> Xi'an Research Institute of Surveying and Mapping, Xi'an 710054, Shanxi, China – qxianping@126.com

Commission IV, WG IV/5

**KEY WORDS:** GNSS-A, Seafloor Geodesy, Positioning, Sound velocity, Temporal and spatial variation, B-Spline.

### ABSTRACT:

The spatial and temporal change of sound speed has a significant impact on the accuracy of GNSS-A underwater positioning. However, it is hard to collect enough data to cover all the spatial and temporal changes of sound velocity. We built an acoustic ranging model that included the sound velocity component, and then we looked at how the model could be used for three-dimensional seabed location and undersea crust monitoring. Meanwhile, B-spline curves are used to construct a sound velocity model that encompasses temporal variation as well as two-dimensional spatial gradients. The method was utilized to assess the simulated data and the in-situ data collected in July 2019, respectively. Simulation results show that the root mean square of the horizontal coordinates solved by the ranging model is less than 10cm, and the model may meet the demands of subsea crust monitoring under certain situations. In the real data experiment, the square root of variance of the coordinate was better than 10 cm. The sound velocity model findings indicated that the variance of sound velocity in the experimental marine region was less than 1m/s, with clear daily patterns and short-period variations. The algorithm does not need the sound velocity profile information and can save the measurement time of the sound velocity profile.

### 1. INTRODUCTION

Due to the severe attenuation of electromagnetic waves underwater, GNSS-A (Global Navigation Satellite System-Acoustic Ranging Combined), which extends the observation network to the seafloor, was proposed and developed (Spiess, F., 1980; Xu et al., 2005; Ikuta et al., 2008; Chen, 2014; Yang, Qin, 2021). The GNSS-A observation system consists of a surface unit (usually a vessel or buoy) and a subsurface transponder. The surface unit is equipped with a GNSS antenna, a vessel attitude sensor, and a ship bottom transducer, allowing real-time location of the surface unit based on the International Terrestrial Reference Frame ITRF and dynamic GNSS. During one measurement, the transponder receives the signal emitted by the transducer and sends the sound signal back to the transducer, then observers will obtain the transmission time by correlating the emitted and received signals. After that, the subsea transponder's coordinates can be determined by establishing the ranging equation with the ocean sound velocity structure. (Yokota et al., 2018b; Ishikawa et al., 2020).

Eliminating systematic errors in acoustic ranging is essential for achieving greater positioning precision of subsea transponders. Generally, system errors include hardware time delays, inaccuracies in sound velocity, and other measurement errors caused by the complicated maritime environment. To reduce or counteract systematic errors in underwater measurement, SIO fixed configurations (the surface unit is roughly in the horizontal center of three or four subsea transponders) and symmetric walk-away configurations are widely used. (Spiess et al., 1998; Obana et al., 2000; Osada et al., 2003; Kido et al., 2006; Kido et al., 2008a; Fujimoto, 2014; Tomita et al., 2017). Both configurations are based on the premise that the systematic error is approximate at the symmetry point, with the horizontal coordinates of the

solitary underwater point or the transponder array's center remaining unaffected by default.

The difference method is a good strategy for reducing systematic error, and it can be used to obtain the seabed transponder position with cm-level precision (Xu et al., 2005; Chen et al., 2020). However, as some scholars have pointed out, the ill-conditioned problem that occurred in the difference equation will result in a poor estimation of the vertical coordinate (Yang, Qin, 2021), which is ineffective for solving the three-dimensional location of the seabed transponder.

In contrast to the linear propagation of electromagnetic waves, the propagation of acoustic signals underwater follows Snell's law of reflection and curved route, especially when acoustic incidence angles are considerable. Some researchers attempted to improve seafloor positioning accuracy by using acoustic ray tracking algorithm and developed some exact equations for calculating sound line tracking time (Dosso, Stan, 1998; Yan, 1999; Zielinski, 1999; Lu et al., 2012). This technique based on the physical properties of acoustic waves can reduce the residual series of the observation equation to some extent, but it needs sound velocity profile data and presupposes that the sound velocity does not fluctuate in the horizontal direction (horizontal stratification of the sound velocity profile). The acoustic tracking algorithm still does not effectively tackle the problem of spatial and temporal variation of sound velocity, and it is incapable of meeting the high-precision positioning requirements when processing actual measurement data (Kido et al., 2008b; Tomita et al., 2019). Seasonal fluctuations, daily variations induced by temperature, and short-period variations caused by internal waves all contribute to the temporal variability of sound velocity. Spatial differences of sound velocity appear as horizontal inhomogeneities due to anomalous seawater advection caused by

\* Corresponding author

internal waves or ocean currents, which are usually found in the ocean's shallower waters (Honsho et al., 2019). The introduction of a time-dependent parameter associated with sound velocity in the ranging equation can significantly improve localization precision (Fujita et al., 2006; Ikuta et al., 2008; Kido et al., 2008a; Honsho, Kido, 2017), and all of these studies can derive the temporal variation of underwater sound velocity concerning a fixed sound velocity profile. The distance-dependent linear model has been demonstrated to be useful in solving the horizontal gradient of the sound velocity while also allowing for flexible depth control. Under specific conditions, the continuous variation of the horizontal gradient can be derived by modeling in the time domain. (Yasuda et al., 2017; Yokota et al., 2018a; Kinugasa et al., 2020; Watanabe et al., 2020).

In the multi-sensor experiment for 3d positioning, the horizontal position of the seabed station is determined by GNSS-A underwater positioning and the vertical position is determined by the pressure sensor (Liu et al., 2019), which increases the difficulty of unifying the seabed station with the global framework. Meanwhile, algorithms using sound velocity profiles may take a long time to process a large number of data with the acoustic ray tracking technique. When only acoustic sensors are available, we hope to get the transponder's three-dimensional position by constructing a simple sound velocity model. Therefore, the speed of sound will be solved as an unknown parameter if the angle of measurement incidence changes dramatically. The method without sound velocity profile has been validated in shallow waters for 3d positioning with a precision better than 5cm (Yang et al., 2011). To prevent frequent measurements of sound velocity, linear and bilinear models are proposed to take into account the fluctuation of sound velocity with depth (Chen, 2014). The model including the offset error of transceiver lever arms is also utilized to improve positioning performance with a precision of better than 1cm (Chen et al., 2019). Subsequently, some scholars extend the equation with time bias and adopt an elastic approach to describe the system error more flexibly by modeling the residuals (Yang, Qin, 2021). All of the approaches discussed above can significantly improve seabed positioning precision; however, few studies on the outer precision of positioning results have been conducted since accurate values of seabed transponder coordinates are difficult to get by other technical means.

Some characteristics of ocean currents can be mirrored in the spatial and temporal variation of sound velocity, particularly the two-dimensional horizontal gradient. In general, the structure of ocean sound velocity parallel to ocean current is more spatially homogenous than that perpendicular to it (Yada et al., 2004). The relationship between continuous horizontal gradients at different depths and the real ocean field was investigated (Yokota, Ishikawa, 2019). The findings showed that the gradient field might respond to the Kuroshio flow (a warm current flowing from the Philippine Sea east of Taiwan to Japan). This indicates that GNSS-A technology may be utilized for more than only seabed transponder positioning; the ocean gradient field derived from acoustic data can also be used to determine the ocean current route. This enables more research into the physical properties of the water.

In this paper, we estimate the spatial and temporal variation of sound velocity using cubic B-spline curves based on a model including the sound velocity parameter, and then we analyze simulated data to demonstrate the model's effectiveness in acoustic positioning. Finally, the coordinate of transponder and sound velocity structure are estimated using acoustic data at a depth over 3000m collected in July 2019. The acoustic ranging equation is presented in section 2 and the sound velocity model based on the cubic B-spline curve is proposed in section 3.

Section 4 provides the calculation and analysis of the simulated and measurement data, and the conclusion is given in Section 5.

## 2. ACOUSTIC RANGING EQUATION AND COLLINEARITY PROBLEM

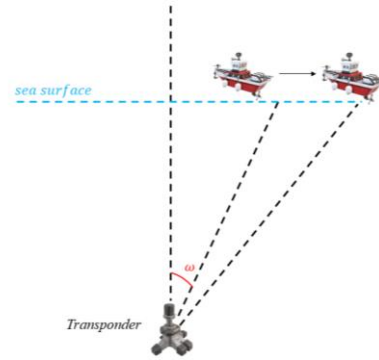


Figure 1. Acoustic observational model.

Acoustic ranging model with sound velocity parameter can be expressed as:

$$\rho_i = f(X_{s0}, X_p) + f(X_{s1}, X_p) + \Delta C \tau_i + \varepsilon_i \quad (1)$$

$$f(X_s, X_p) = \sqrt{(x_s - x_p)^2 + (y_s - y_p)^2 + (z_s - z_p)^2} \quad (2)$$

where  $\rho_i$  = the ranging between the transponder on the seafloor and the transducer under the ship at epoch  $i$   
 $f(X_s, X_p)$  = the theoretical distance between the transducer  $X_{s0}$  and the transponder  $X_p$  at the epoch of signal transmission.  
 $f(X_s, X_p)$  = the theoretical distance between the transducer  $X_{s1}$  and the transponder  $X_p$  at the epoch of signal receiving.  
 $\Delta C$  = the sound speed bias  
 $\tau_i$  = the travel time at epoch  $i$   
 $\varepsilon_i$  = the random ranging error

Linearizing the observation equation:

$$V = AdX - L \quad (3)$$

$$F = f(X_{s0}, X_p) + f(X_{s1}, X_p) \quad (4)$$

$$A = \begin{bmatrix} \frac{\partial F_1}{\partial x} & \frac{\partial F_1}{\partial y} & \frac{\partial F_1}{\partial z} & -\tau_1 \\ \vdots & \vdots & \vdots & \vdots \\ \frac{\partial F_n}{\partial x} & \frac{\partial F_n}{\partial y} & \frac{\partial F_n}{\partial z} & -\tau_n \end{bmatrix} \quad (5)$$

$$L = [C_0 \tau_1 - F_1 \dots C_0 \tau_n - F_n]^T \quad (6)$$

where  $dX$  = the correction of parameters (3D coordinates and sound velocity)  
 $A$  = the coefficient matrix of observation equation  
 $V$  = the observation residual vector  
 $C_0$  = Initial value of sound velocity  
 $n$  = the number of observations

To achieve optimal unbiased parameter estimation in linear models, the Gauss-Markov theorem is commonly used to estimate unknown parameters:

$$dX = (A^T P A)^{-1} A^T P L \quad (7)$$

$$\hat{X} = X_0 + dX \quad (8)$$

$$D_{\hat{X}\hat{X}} = \sigma_0^2 Q_{\hat{X}\hat{X}} = \sigma_0^2 (A^T P A)^{-1} \quad (9)$$

$$\sigma_0^2 = \frac{V^T P V}{n - 4} \quad (10)$$

where  $P$  = the weight matrix of observations (an equal weight assumption is used in this paper)  
 $D_{\hat{X}\hat{X}}$  = the covariance matrix of unknown parameters.  
 $\sigma_0^2$  = the variance of unit weight  
 $V$  = the observation residual vector.  
 $Q_{\hat{X}\hat{X}}$  = the cofactor matrix of unknown parameters

Eq. (7) is based on the assumption that the parameters are linearly independent, and thus cannot offer an adequate estimate when the parameters are highly correlated with one another. In that case, the determinant of  $A^T P A$  approaches zero, making the solution extremely unstable and leading to erroneous statistical results. The co-linear relationship of parameters is usually caused by defects in the data or over-parameterization of the model, and the performance indicators of the coefficient matrix may be used to analyze the correlation of parameters. We studied the circle configuration and crossover configuration for seafloor positioning, as shown in Fig. 2, for both configurations:

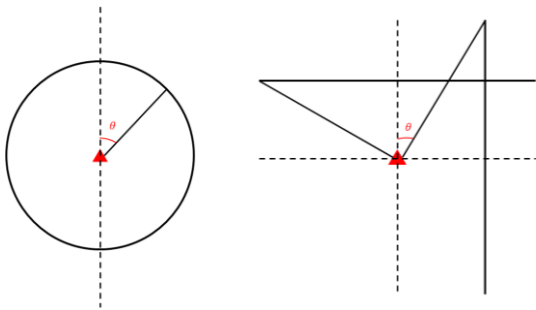


Figure 2. Geometric configuration.

$$A = \begin{bmatrix} \cos\theta_1 \cdot \sin\omega_1 & \sin\theta_1 \cdot \sin\omega_1 & \cos\omega_1 & -\tau_1 \\ \vdots & \vdots & \vdots & \vdots \\ \cos\theta_n \cdot \sin\omega_n & \sin\theta_n \cdot \sin\omega_n & \cos\omega_n & -\tau_n \end{bmatrix} = [A_1 \ A_2 \ A_3 \ A_4] \quad (11)$$

where  $\theta$  = the azimuth angle of the line between transponder and transducer onto the horizontal plane  
 $\omega$  = the inclination angle between the zenith and the line of sight from the transducer to the transponder (shown in Fig. 1)

For circle track, It is obvious that there exists  $k = \cos\omega_n / \tau_n$  such that  $A_3 + k \cdot A_4 = 0$ , implying that the coefficient matrix is not full column rank, and the vertical coordinate parameter is linearly related to the sound velocity parameter. The correlation of all parameters is shown in Fig. 3.

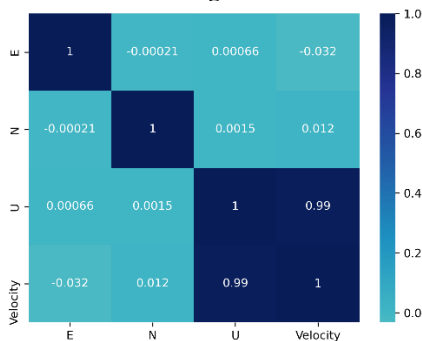


Figure 3. Parameter correlation of circle configuration.

As shown in Fig. 4, because of greater variation of  $\tau_n$ , the performance of the coefficient matrix for the cross configuration is better than circle configuration, but these two parameters are still highly correlated.

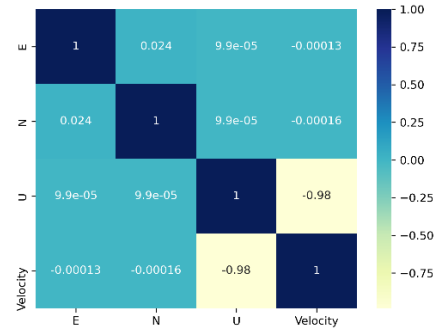


Figure 4. Parameter correlation of cross configuration.

Bayesian estimation, ridge estimation, and other methodologies such as principal component analysis are extensively used for the solution of ill-condition equations (Massy, 1965; Mandel, 1982; Marin, Robert, 2007). These methods effectively address the problem by providing external information or reducing dimensionality. It should be noted that the linear combination of strongly correlated parameters may be accurately estimated in the collinearity problem, while collinearity has no effect on the estimation of other uncorrelated parameters. This means that if the variation range of sound velocity is controlled, the vertical coordinates of the seafloor transponder will be quite stable, which is advantageous for monitoring the vertical displacement of the seafloor crust.

### 3. SOUND VELOCITY PERTURBATION MODEL

Because of the spatial and temporal variation of the sound speed, the residuals of Eq. (3) will include periodic systematic errors that directly represent the sound speed fluctuation. The time-continuous property of the sound speed perturbation can be satisfied by b-spline curves; however, if the temporal and spatial variation of the sound speed is estimated simultaneously, the smoothness of the curve must be controlled by hyperparameters for the collinearity problem caused by the over-definition model (Ikuta et al., 2008; Watanabe et al., 2020). On the other hand, this method can also improve positioning precision as a resilient way for modeling systematic errors (Yang, Qin, 2021). Cubic B-spline curve model constructed on  $n+1$  nodes may be expressed as the following equation to derive the temporal variation of the sound velocity and the two-dimensional spatial gradient:

$$v_i = A_i d\hat{X}_p + \Delta \hat{C} \tau_i - (\rho_i - \rho_i^0) \quad (12)$$

$$v_i = \tau_i \left( \sum_{i=0}^n a_1 B_{i,3}(t_*) + \sum_{i=0}^n a_2 B_{i,3}(t_*) * d \cos\varphi + \sum_{i=0}^n a_3 B_{i,3}(t_*) * d \sin\varphi \right) \quad (13)$$

$$t_* = \frac{t - t_i}{t_{i+1} - t_i} \quad t \in (t_i, t_{i+1}) \quad (14)$$

where  $v_i$  = the residuals of Eq. (3)  
 $a_1$  = time-varying parameter of sound velocity  
 $a_2, a_3$  = two-dimensional spatial gradient  
 $B_{i,3}(t_*)$  = cubic B-spline basis function  
 $\varphi$  = the azimuth angle of the transducer relative to the transponder.

Eq. (13) containing three kinds of parameters is to be solved by least squares with constraints. To control the roughness of the

curve, the integral of the second-order derivative of the B-spline curve basis function is used as the a priori weight matrix of the sound velocity perturbation parameters(Honsho, Kido, 2017; Watanabe et al., 2020), which can be adjusted by the hyperparameters.

$$P_{i,j} = \mu \int \frac{\partial^2 B_{i,3}(t)}{\partial t^2} \frac{\partial^2 B_{j,3}(t)}{\partial t^2} dt \quad (15)$$

$$P_0 = \text{diag}(P_{i,j} \ 10^2 P_{i,j} \ 10^2 P_{i,j}) \quad (16)$$

$$a = (E^T E + P_0)^{-1} (E^T v) \quad (17)$$

where  $P_0$  = Prior weight matrix (set the weight matrices of  $a_2$  and  $a_3$  to be two orders of magnitude larger than the weight matrix of  $a_1$ , implying that the spatial variation is smoother.)

$E$  = the Jacobi matrix of Eq. (13) for all sound velocity parameters.

By this way, the temporal variation and horizontal spatial gradient of oceanic sound speed can be derived, and the horizontal spatial variation may have the capacity to reflect the flow route of ocean currents.

#### 4. DATA CALCULATION AND ANALYSIS

##### 4.1 Analysis of simulation data

The measured sound velocity profile of 3000m and sound ray tracking technique are used to simulate the acoustic signal's travel time. The speed of ship is 3 knots per hour and the sample interval is 12.4 seconds for simulating acoustic observation data. The long and short periods of sound velocity change are set to 90 minutes and 24 hours, respectively. The effect of changing sound velocity on measurement time is simulated based on the following equation:

$$\Delta V_i = c_1 \sin\left(\frac{2(t-t_0)}{T_s} \pi\right) + c_2 \sin\left(\frac{2(t-t_0)}{T_L} \pi\right) \quad (18)$$

$$\tau_i = \frac{S_i}{V_i + \Delta V_i} \quad (19)$$

where  $c_1 = 0.13\text{m/s}$

$c_2 = 0.4\text{m/s}$

$S_i$  = Actual acoustic path length

$V_i$  = sound velocity calculated by velocity profile

Considering the influence of the ship track geometry configuration on the positioning accuracy(Sato et al., 2013; Zhao et al., 2016; Xue, Yang, 2017), one circular track with a radius of about 1.5 times the water depth and cross track are used for simulation experiments. The spatial location of the transponder and sampled data are shown in Fig. 5.

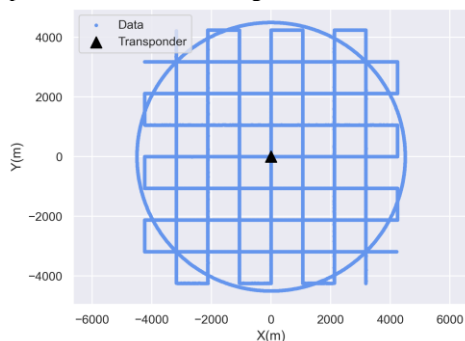


Figure 5. Spatial position.

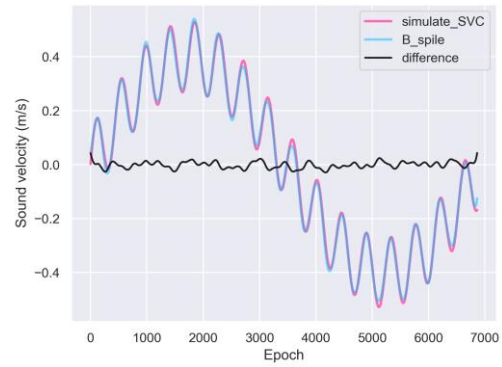


Figure 6. Sound speed setting and estimation.

Data	Coordinates			Root mean squares (RMS)		
	E(m)	N(m)	U(m)	(cm)	(cm)	(cm)
Cross	-0.005	0.039	-3000.333	0.5	3.9	33.3
Circle	0.035	-0.016	-2329.809	3.5	1.6	67019.1
Circle + control	0.039	-0.013	-3000.214	3.9	1.3	21.4

Table 1. Positioning results of simulation data.

Table 1 shows the location results using simulated data. Given the significant correlation of the circle configuration, the circle data is separated into two instances for computation based on whether the sound speed limitation is included or not, circle with control is limited by introducing the average sound speed calculated from the Cross data. The root mean square (RMS) of the horizontal coordinates solved for all data is better than 5 cm. Due to the collinearity of the circle data without constraints, positioning parameters have a large departure from the truth value of its vertical coordinates, but the vertical location result of the circle data with the constraint of sound velocity is similar to cross, both of which are of the level of decimetres. It is also worth noting that, in the circular walk configuration, the presence or lack of vertical information does not affect the estimate of horizontal coordinates, implying that collinearity has no effect on the estimation of uncorrelated parameters.

The point of Fig. 6 is to compare sound speed simulation to sound speed estimation of cross data, with the red line representing the simulated sound speed perturbation, the blue line showing sound speed perturbation estimated by B-spline, and the black line reflecting the difference between the two. It can be seen that the two have a high degree of agreement, indicating that the functional model's residual series completely reacts to the fluctuation of the sound velocity and proving the superiority of the B-spline curve for the estimation of continuous variation regarding time series.

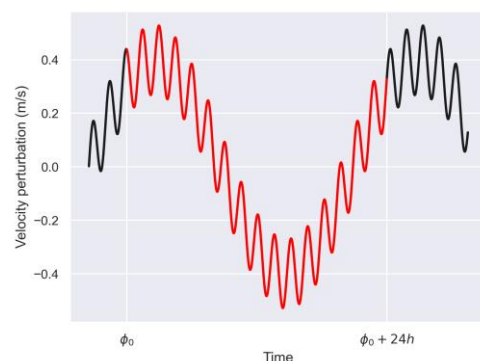
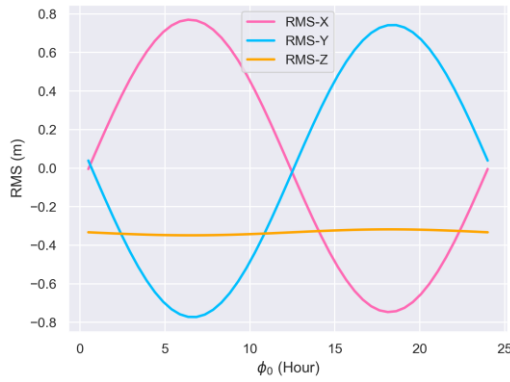


Figure 7. Phase simulator.



**Figure 8.** The change of coordinate with phase.

We also analyzed the influence of varying sound velocity's initial phase on coordinates solved by the cross configuration. One cycle of sound velocity fluctuation with different beginning phases (0 to 24 hours) is established, as illustrated in Fig. 7. The change of the root mean square of horizontal and vertical coordinates with the initial phase is shown in Fig. 8. It can be seen that the horizontal coordinate is greatly influenced, with a maximum mutual difference of 1.6m for one cycle, but the vertical coordinates are quite stable, with an overall fluctuation of less than 3cm. Because sound velocity in the ocean has obvious time-varying and weak spatially varying characteristics, it is nearly impossible to guarantee the same sound velocity structure at the symmetry points in the actual measurement, which will almost certainly result in a horizontal coordinate offset, and the magnitude of the offset is related to the initial phase of the sound velocity change. The strong correlation between the sound velocity parameters and the vertical coordinates, on the other hand, provides us with a method of solving the stable transponder vertical coordinates: it is just essential to ensure that a complete period (typically roughly 24 hours) is observed, without focusing on the initial moment of measurement. This is significant for monitoring the seafloor crust since it is concerned with stability rather than the accuracy of the vertical coordinates. Although the results shown in Table 1 indicates that the transponder vertical coordinates calculated using cross data differ from the truth value by 33.3 cm, the experiments in Fig. 8 imply that the technique can detect vertical seabed displacements greater than 3 cm.

#### 4.2 Analysis of in-situ data

From July 14 to 16, 2019, an acoustic localization experiment for one seabed transponder at 3000 m water depth was carried out. The experiment involved three observation configurations. Fig. 9 displays the horizontal spatial link between the seabed transponder and the observation data, where the yellow line corresponds to data Data1, the red line to data Data2, and the blue line to data Data3. Table 2 shows the complete information for these three data sets, and it is noticeable that they are observations from separate periods, allowing their results to be compared. Data3 is not a continuous data set, having gaps of 3 or 4 hours between periods. Theoretically, the more B-spline time nodes sampled in a continuous period, the better the modeling results, but there may be a risk of overfitting. Time nodes are taken at 30min intervals in this article, and the number of period nodes is proportionate to the duration of observation.

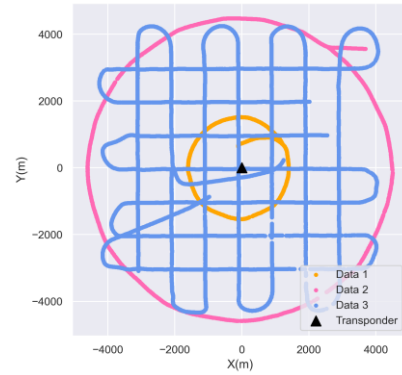


**Figure 9.** The spatial position of observation data.

Section	Number of segments	Time	Number of observations
Data 1	1	15.81-15.88	514
Data 2	1	16.12-16.29	1119
Data 3	3	14.86-15.15	1889
		15.28-15.71	2884
		15.88-15.98	697

**Table 2.** Information of observation data.

The circular data (Data1/2) are processed in two ways: normally (Table 3), and with the sound speed constraint calculated by Data3 (Table 4).

As shown in Table 3, the greatest differences in the E/N/U components across different data sets are 0.478, 0.031, and 4.931 m. The collinearity of the model results in very poor repetition of the U component, whereas the inferior repetition of the E coordinate is thought to be owing to the same circumstance as in Fig. 8. In other words, the sound velocity structure of Data3 results in a slower average sound velocity on the west side of the transponder than on the east side, with no significant difference between the north and south sides.

After residual modeling, the square root of variance of all coordinates was better than 10 cm. The 3D coordinates with the best precision are those calculated from the Data3 with the longest observation time. Meanwhile, the horizontal coordinate precision of Data2 with a radius of 1.5 times the sea depth is better than that of Data1, which is compatible with the results of studies about geometric configuration (Zhao et al., 2016; Xue, Yang, 2017; Chen et al., 2020).

Data set	Coordinates			Square root of variance		
	E(m)	N(m)	U(m)	$m_E$ (cm)	$m_N$ (cm)	$m_U$ (cm)
Data 1	0.504	0.445	0.254	7.7	7.7	2.6
Data 2	0.578	0.453	-4.195	5.3	5.3	5.5
Data 3	0.100	0.422	0.736	2.7	2.6	1.7

**Table 3.** Calculate normally.

Data set	Coordinates			Square root of variance		
	E(m)	N(m)	U(m)	$m_E$ (cm)	$m_N$ (cm)	$m_U$ (cm)
Data 1	0.483	0.432	0.617	7.7	7.7	2.6
Data 2	0.487	0.393	3.183	5.3	5.3	5.5
Data 3	0.100	0.422	0.736	2.7	2.6	1.7

**Table 4.** Calculate with sound speed constraint.

The horizontal coordinates and precision do not vary considerably after introducing the sound velocity restriction, as shown in Table 4, however, the vertical coordinates of the circle data (Data1/2) differ dramatically from the previous ones. It can be seen that the vertical coordinates of Data1 and Data2 are both closer to the vertical coordinate of Data3, but Data2 is still a long

way from the truth value. This phenomenon might be attributed to two factors: (1) The speed of sound solved by Data3 differs much from the real sound speed along Data2's sound path. (2) As shown by the yellow line in Fig. 9, Data1 is not precise circle data, with a tiny fraction of its track points near to the center of the circle, making the vertical coordinate calculated by Data1 closer to the true value.

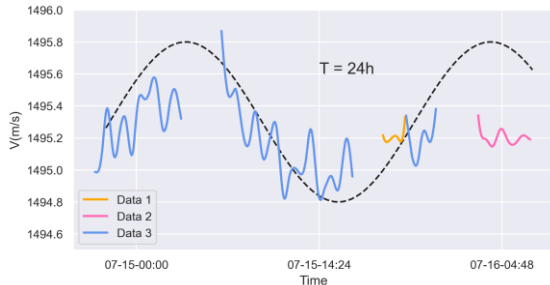


Figure 10. Time variation of the sound speed.

Fig. 10 shows the estimated sound velocity variation, which has a clear trend of daily variation and short-period fluctuations similar to internal waves, and the total temporal variation of sound velocity is less than 1 m/s. The red line (Data2) is clearly out of the black sine curve, which is related to the poorer vertical coordinates obtained from the Data2 solution. As shown in Fig. 11, fixing the 2D spatial gradient directly with B splines is not feasible because the local poor geometric design leads to local mistakes of spatial gradient inversion. These scenarios occur when the bottom transducer is close to the transponder for an extended period (black dashed box), and the horizontal distance approximating zero is insufficient to hold the sound velocity information. Therefore, we tighten the constraint and force the spatial gradient to remain constant during the observation. As illustrated in Fig. 12, The east-west spatial gradient attained is 0.006 m/s/km, and the north-south spatial gradient is 0.028 m/s/km. The more active north-south sound velocity structure during the observation might imply the presence of east-west currents inside the ocean.

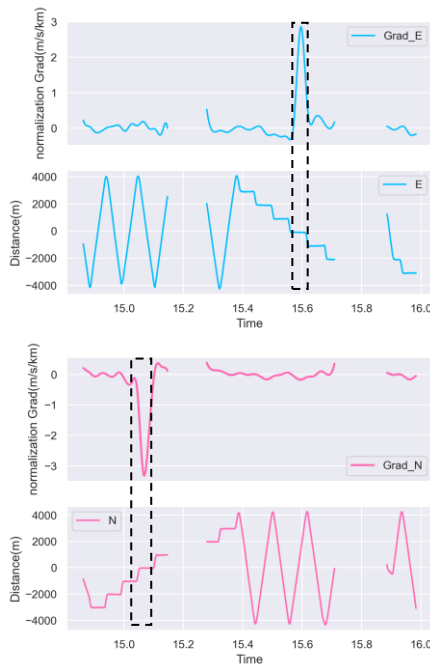


Figure 11. Horizontal distance from the transducer to the transponder and spatial gradient.

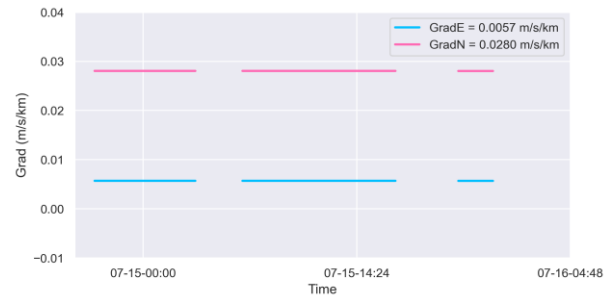


Figure 12. 2D spatial gradient with constraint.

## 5. CONCLUSION

The model with sound velocity parameter can be used to obtain three-dimensional seafloor transponder coordinates, and the cross track is beneficial for the vertical coordinate estimation. After the spatial and temporal variation of the sound speed was estimated, the square root of variance of the coordinate was better than 10 cm.

For circle track, the sound velocity parameters are linearly correlated with the vertical coordinate parameters, which will lead to poor vertical coordinate estimation, but this does not affect the horizontal coordinate estimation. For cross track, the sound velocity parameters are strongly correlated with the vertical coordinate parameters, which is beneficial for the vertical displacement monitoring of the submarine crust. The simulation experiment showed that the seafloor vertical displacement larger than 3 cm could be detected as long as one cycle of observation was guaranteed.

The residuals reflect the fluctuation of the sound velocity. The situ data showed that the variation of sound velocity in the experimental sea area was less than 1 m/s, and it had obvious daily trends and short-period fluctuations. Meanwhile, the north-south sound velocity gradient was more active than the east-west sound velocity gradient, which might imply the existence of east-west currents in the sea area during the observation period.

## ACKNOWLEDGEMENTS

This research is financially supported by Wenhai Program of the S&T Fund of Shandong Province for Pilot National Laboratory for Marine Science and Technology (Qingdao) (NO. 2021WHZZB1004), and the National Key Research & Development Program of China (2020YFB0505804).

## REFERENCES

- Chen, G., Liu, Y., Liu, Y., Liu, J. 2020. Improving GNSS-acoustic positioning by optimizing the ship's track lines and observation combinations. *Journal of Geodesy*, 94 (6): 61.
- Chen, G., Liu, Y., Liu, Y., Tian, Z., Li, M. 2019. Adjustment of Transceiver Lever Arm Offset and Sound Speed Bias for GNSS-Acoustic Positioning. *Remote Sensing*, 11 (13): 1606.
- Chen, H. H. 2014. Travel-time approximation of acoustic ranging in GPS/Acoustic seafloor geodesy. *Ocean Engineering*, 84: 133-144.
- Dosso, Stan, E. 1998. Array element localization for horizontal arrays via Occam's inversion. *Acoustical Society of America Journal*, 104 (2): 846-859.

- Fujimoto, H. 2014. Seafloor Geodetic Approaches to Subduction Thrust Earthquakes. *monographs on environment earth & planets meep*.
- Fujita, Masayuki, Ishikawa, Tadashi, Mochizuki, Masashi, Sato, Mariko, Toyama, Shin-Ichi, Katayama, Masato, Kawai, Koji, et al. 2006. GPS/Acoustic seafloor geodetic observation: method of data analysis and its application. *Earth, Planets and Space*, 58 (3): 265-275.
- Honsho, C., Kido, M., Tomita, F., Uchida, N. 2019. Offshore Postseismic Deformation of the 2011 Tohoku Earthquake Revisited: Application of an Improved GPS - Acoustic Positioning Method Considering Horizontal Gradient of Sound Speed Structure. *Journal of Geophysical Research: Solid Earth*, 124 (6).
- Honsho, Chie, Kido, Motoyuki. 2017. Comprehensive Analysis of Traveltime Data Collected Through GPS-Acoustic Observation of Seafloor Crustal Movements. *Journal of Geophysical Research: Solid Earth*, 122 (10): 8583-8599.
- Ikuta, Ryoya, Tadokoro, Keiichi, Ando, Masataka, Okuda, Takashi, Sugimoto, Shingo, Takatani, Kazunori, Yada, Kazuyuki, Besana, Glenda M. 2008. A new GPS-acoustic method for measuring ocean floor crustal deformation: Application to the Nankai Trough. *Journal of Geophysical Research*, 113 (B2).
- Ishikawa, T., Yokota, Y., Watanabe, S. I., Nakamura, Y. 2020. History of On-Board Equipment Improvement for GNSS-A Observation With Focus on Observation Frequency. *Frontiers in Earth Science*, 8: 150.
- Kido, M., Osada, Y., Fujimoto, H. 2008a. Temporal variation of sound speed in ocean: a comparison between GPS/acoustic and in situ measurements. *Earth Planets & Space*, 60 (3): 229-234.
- Kido, Motoyuki, Fujimoto, Hiromi, Miura, Satoshi, Osada, Yukihito, Tsuka, Kentaro, Tabei, Takao. 2006. Seafloor displacement at Kumano-nada caused by the 2004 off Kii Peninsula earthquakes, detected through repeated GPS/Acoustic surveys. *Earth, Planets and Space*, 58 (7): 911-915.
- Kido, Motoyuki, Osada, Yukihito, Fujimoto, Hiromi. 2008b. Temporal variation of sound speed in ocean: a comparison between GPS/acoustic and in situ measurements. *Earth, Planets and Space*, 60 (3): 229-234.
- Kinugasa, Natsuki, Tadokoro, Keiichi, Kato, Teruyuki, Terada, Yukihito. 2020. Estimation of temporal and spatial variation of sound speed in ocean from GNSS-A measurements for observation using moored buoy. *Progress in Earth and Planetary Science*, 7 (1).
- Liu, J., Chen, G., Zhao, J., Gao, K., Liu, Y. 2019. Development and Trends of Marine Space-Time Frame Network. *Wuhan Daxue Xuebao (Xinxi Kexue Ban)/Geomatics and Information Science of Wuhan University*, 44 (1): 17-37.
- Lu, X., Bian, S., Huang, M., Zhai, G. 2012. An Improved Method for Calculating Average Sound Speed in Constant Gradient Sound Ray Tracing Technology. *Geomatics and Information Science of Wuhan University*, 37 (5): 590-593.
- Mandel, J. 1982. Use of the Singular Value Decomposition in Regression Analysis. *American Statistician*, 36 (1): 15-24.
- Marin, J. M., Robert, C. P. 2007. *Bayesian Core* (Bayesian Core).
- Massy, William F. 1965. Principal Components Regression in Exploratory Statistical Research. *Publications of the American Statistical Association*, 60 (309): 234-256.
- Obana, K., Katao, H., Ando, M. 2000. Seafloor positioning system with GPS-acoustic link for crustal dynamics observation—a preliminary result from experiments in the sea—. *Earth Planets & Space*, 52 (6): 415-423.
- Osada, Y., Fujimoto, H., Miura, S., Sweeney, A., Kanazawa, T., Nakao, S., Sakai, S. I., Hildebrand, J. A., Chadwell, C. D. 2003. Estimation and correction for the effect of sound velocity variation on GPS/Acoustic seafloor positioning: An experiment off Hawaii Island. *Earth, Planets & Space*.
- Sato, M., Fujita, M., Matsumoto, Y., Saito, H., Ishikawa, T., Asakura, T. 2013. Improvement of GPS/acoustic seafloor positioning precision through controlling the ship's track line. *Journal of Geodesy*, 87 (9): 825-842.
- Spiess, F., N. 1980. Acoustic techniques for Marine Geodesy. *Marine Geodesy*, 4 (1): 13-27.
- Spiess, F. N., Chadwell, C. D., Hildebrand, J. A., Young, L. E., Purcell, George H, Dragert, H. 1998. Precise GPS/Acoustic positioning of seafloor reference points for tectonic studies. *Physics of the Earth & Planetary Interiors*, 108 (2): 101-112.
- Tomita, F., Kido, M., Honsho, C., Matsui, R. 2019. Development of a kinematic GNSS-Acoustic positioning method based on a state-space model. *Earth, Planets and Space*, 71 (1).
- Tomita, F., Kido, M., Ohta, Y., Iinuma, T., Hino, R. 2017. Along-trench variation in seafloor displacements after the 2011 Tohoku earthquake. *Science Advances*, 3 (7): e1700113.
- Watanabe, S. I., Ishikawa, T., Yokota, Y., Nakamura, Y. 2020. GARPOS: analysis software for the GNSS-A seafloor positioning with simultaneous estimation of sound speed structure. *Frontiers in Earth Science*, 8 (2296-6463).
- Xu, P., Ando, M., Tadokoro, K. 2005. Precise, three-dimensional seafloor geodetic deformation measurements using difference techniques. *Earth, Planets and Space*, 57 (9): 795-808.
- Xue, S, Yang, Y. 2017. Understanding GDOP minimization in GNSS positioning: Infinite solutions, finite solutions and no solution. *Advances in Space Research*, 59 (3): 775-785.
- Yada, K., Ikuta, R., Ando, M., Okuda, T., Takatani, K. 2004. Spatial variations in Acoustic velocity at Kuroshio region for the accurate ocean-bottom positioning. *AGU Fall Meeting Abstracts*.
- Yan, J. 1999. Effects of earth curvature on two-dimensional ray tracing in underwater acoustics. *Applied Acoustics*, 57 (2): 163-177.
- Yang, F., Lu, X., Li, J., Han, L., Zheng, Z. 2011. Precise Positioning of Underwater Static Objects without Sound Speed Profile. *Marine Geodesy*, 34 (2): 138-151.
- Yang, Y., Qin, X. 2021. Resilient observation models for seafloor geodetic positioning. *Journal of Geodesy*, 95 (7): 1-13.

Yasuda, K., Tadokoro, K., Taniguchi, S., Kimura, H., Matsuhira, K. 2017. Interplate locking condition derived from seafloor geodetic observation in the shallowest subduction segment at the Central Nankai Trough, Japan. *Geophysical Research Letters*, 44 (8): 3572-3579.

Yokota, Y., Ishikawa, T. 2019. Gradient field of undersea sound speed structure extracted from the GNSS-A oceanography: GNSS-A as a sensor for detecting sound speed gradient. *SN Applied Sciences*, 1 (7).

Yokota, Y., Ishikawa, T., Watanabe, S. I. 2018a. Gradient field of undersea sound speed structure extracted from the GNSS-A oceanography. *Marine Geophysical Researches*.

Yokota, Yusuke, Ishikawa, Tadashi, Watanabe, Shun-Ichi. 2018b. Seafloor crustal deformation data along the subduction zones around Japan obtained by GNSS-A observations. *Scientific Data*, 5 (1): 180-182.

Zhao, J., Zou, Y., Zhang, H., Wu, Y., Fang, S. 2016. A new method for absolute datum transfer in seafloor control network measurement. *Journal of Marine Science & Technology*, 21 (2): 216-226.

Zielinski, Xueyi Geng Adam. 1999. Precise Multibeam Acoustic Bathymetry. *Marine Geodesy*, 22 (3): 157-167.